The University of Bradford Institutional Repository

http://bradscholars.brad.ac.uk

This work is made available online in accordance with publisher policies. Please refer to the repository record for this item and our Policy Document available from the repository home page for further information.

To see the final version of this work please visit the publisher's website. Access to the published online version may require a subscription.

Polymorphism in sulfadimidine/4-aminosalicylic acid cocrystals: solid state characterization and physicochemical properties

C. Grossjohann[a], D. R. Serrano[a], K. J. Paluch[a], P. O'Connell[a], L. Vella-Zarb [b], P. Manesiotis[c] T. McCabe[d], L. Tajber[a], O.I. Corrigan [a], A.M. Healy [a,*]

[a] School of Pharmacy and Pharmaceutical Sciences, Panoz Institute, Trinity College Dublin, Dublin, Ireland.

[b] Department of Chemistry, University of Malta, Msida, Malta.

[c] Pharmaceutical and Molecular Biotechnology Research Centre, Waterford Institute of Technology, Waterford, Ireland.

[d] School of Chemistry, Trinity College Dublin, Dublin, Ireland.

*Corresponding author:

Tel.: +353 1 896 1444; fax: +353 1 896 2783.

E-mail address: healyam@tcd.ie (A.M. Healy)

Abstract

Polymorphism of crystalline drugs is a common phenomenon. However, the number of reported polymorphic cocrystals is very limited. In this work, the synthesis and solid state characterisation of a polymorphic cocrystal composed of sulfadimidine (SD) and 4-aminosalicylic acid (4-ASA) is reported for the first time. By liquid-assisted milling, the SD:4-ASA 1:1 form I cocrystal, the structure of which has been previously reported, was formed. By spray drying, a new polymorphic form (form II) of the SD:4-ASA 1:1 cocrystal was discovered which could also be obtained by solvent evaporation from ethanol and acetone. Structure determination of the form II cocrystal was calculated using high resolution X-ray powder diffraction. The solubility of the SD:4-ASA 1:1 cocrystal was dependent on the pH and predicted by a model established for a two amphoteric component cocrystal. The form I cocrystal was found to be thermodynamically more stable in aqueous solution than form II, which showed transformation to form I. Dissolution studies revealed that the dissolution rate of SD from both cocrystals was enhanced when compared to a physical equimolar mixture and pure SD.

Graphical abstract
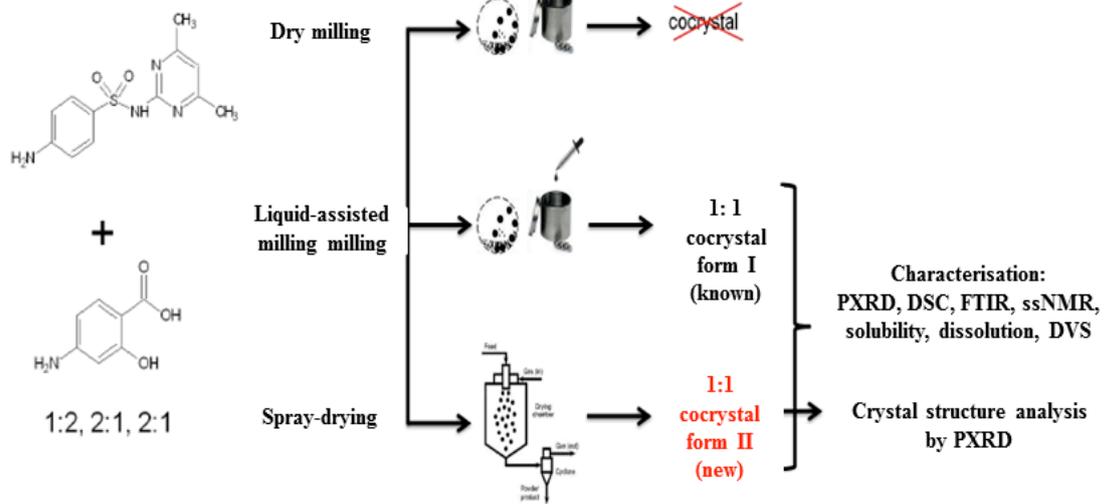
1. Introduction

New pharmaceutical approaches are demanded to enhance the productivity of the pharmaceutical industry which is witnessing an oncoming crisis due to the combined effects of increasing costs for R&D, several blockbuster drugs falling off the patent cliff, decreasing numbers of drugs being approved by the regulatory agencies and numerous drug candidates in the pipeline with poor aqueous solubility [1,2]. The use of salt formation as an approach to improve drug solubility is not always a successful alternative, especially when molecules have no ionisable functional groups or when they are prone to degradation. Engineering of pharmaceutical cocrystals can be an attractive approach for the pharmaceutical industry, since they offer multiple possibilities to modify the physicochemical properties of an API without creating or breaking covalent bonds while still maintaining the intrinsic activity of the drug molecule [3,4]. A major advantage of cocrystal formation is the possibility of transforming a crystalline API into a solid form that exhibits a higher dissolution rate, comparable to that obtained with the amorphous form, while at the same time maintaining the long-term physical and chemical stability of the crystalline API (active pharmaceutical ingredient) [5].

Pharmaceutical cocrystals are generally formed from an API and one or more pharmaceutical compounds (generally regarded as safe – GRAS) known as cocrystal formers or coformers. Molecules that contain multiple hydrogen bond donor and acceptor functions allow for the formation of a diverse range of stable supramolecular motifs in solution, and thereafter the opportunity of cocrystal engineering [6]. Reaction crystallization techniques and grinding are common strategies to produce cocrystals in pharmaceutical companies. Nevertheless, spray drying, a well-established scale-up technique, can be considered as a novel approach in which pure cocrystals can be formed [7].

In spite of the fact that newer antimicrobial drugs have displaced many sulfonamides, their low cost and relatively high efficiency against common bacterial diseases means that they still enjoy relatively widespread use, especially in developing countries [6]. Based on the multiple hydrogen bond donor and acceptor groups of sulfadimidine (SD), cocrystal engineering can be used as an approach, not only to improve its physicochemical properties, but also to exploit a synergistic effect when combined with coformers such as 4-aminosalicylic acid (4-ASA) which possesses anti-inflammatory properties [8] and antibacterial activity, like SD [9]. The formation of the cocrystal composed of one molecule of SD and one molecule of 4-ASA by the solvent evaporation method has been reported by Caira in 1992 [9]. The hypothesis

supporting this work is that spray drying may be used as an alternative production method to prepare the SD:4-ASA cocrystal. The main objective in this study was to investigate cocrystal formation between SD and 4-ASA by grinding, in the form of dry and liquid-assisted milling and by spray drying, followed by comparative solid state characterization and analysis of the physicochemical properties and dissolution profiles of the cocrystal forms prepared.

2. Materials

SD and 4-ASA were purchased from Sigma-Aldrich (Ireland) with a purity $\geq 99\%$. Ethanol and acetone were supplied from Corcoran Chemicals (Ireland). Methanol, HPLC grade, was purchased from Fisher Scientific (Ireland), potassium hydrogen phosphate was obtained from Sigma-Aldrich (Ireland) and phosphoric acid from Merck (Germany). Water, analytical and HPLC grade, was prepared from an Elix 3 connected to a Synergy UV system (Millipore, UK). All other chemicals purchased from commercial suppliers were of analytical grade.

3. Methods

3.1. Preparation of cocrystals and physical mixture of SD:4-ASA

3.1.1. Grinding (dry and liquid-assisted milling)

Dry and liquid-assisted co-milling was carried out for different molar ratios of SD:4-ASA (1:2, 1:1, 2:1) in a Retsch PM100 planetary ball mill (Germany) using three stainless steel balls in each milling jar (50 ml). A maximum of 2.5 g of sample mass was used. In the case of liquid-assisted milling, five drops of ethanol were added to the solid mix prior to milling using a 3.5 ml disposable transfer pipette (Fisher Scientific, Ireland). The milling was carried out at room temperature for 15, 30 and 45 minutes at a rotation speed of 400 rpm. For the milling time of 45 minutes, the milling process was stopped after 30 minutes for 10 minutes in order to avoid a high temperature in the jar and thus the risk of melting/decomposition of the compounds.

3.1.2. Spray drying

Spray drying was performed using a Büchi B-290 Mini Spray Dryer connected to a compressor (HaughTM SO 45E2 ASY) operating in the open-mode. Solution concentrations of 1 % (w/v) of SD:4-ASA in 1:2, 1:1 and 2:1 molar ratio were prepared using ethanol. The

solutions were delivered to a 2-fluid atomization nozzle using a peristaltic pump at a speed of 30 % (9–10 ml/min) and the aspirator was operated at 100%. The flowmeter for the standard 2-fluid nozzle was set at 4 cm which is equivalent to 473 Nl/h (Büchi Labortechnik, Switzerland). The inlet temperature was fixed at 78 °C and the appropriate outlet temperature varied between 50 – 57 °C.

3.1.3. Crystallisation from solution

SD and 4-ASA in 1:1 molar ratio were dissolved in 20 ml of hot ethanol and acetone. The solution was covered with an aluminium foil in which a syringe needle (0.3 x 12mm, Sterican®) was inserted and left for slow evaporation of the solvent, while maintaining the elevated temperature of the solution using an oil bath (70 °C).

3.1.4. Physical mixture

4-ASA and SD in 1:1 molar ratio were manually mixed using a mortar and pestle.

3.2. Solid state characterisation

3.2.1. Powder X-ray diffraction (PXRD)

Powder X-ray analysis was performed using a Miniflex II Rigaku diffractometer with Ni-filtered Cu Kα radiation (λ= 1.54 Å). The tube voltage and tube current used were 30 kV and 15 mA, respectively. Each sample was scanned over a 2 theta range of 5–40 ° with a step size of 0.05°/s. The program Mercury 2.3 [10] was used for calculation of X-ray powder patterns on the basis of the single crystal structure.

3.2.2. Thermal analysis

Differential scanning calorimetry (DSC)

Differential scanning calorimetry was performed using a Mettler Toledo DSC 821e instrument under nitrogen purge. Sample powders (3–5 mg) were placed in aluminium pans, sealed, pierced to provide three vent holes and heated at a rate of 10 ^{0}C/min in the temperature range of 25–225 ^{0}C [11].

Thermogravimetric analysis (TGA)

Thermogravimetric analysis was performed using a Mettler TG 50 module. Samples were placed into open aluminium pans (5–7 mg) and analysed at a constant heating rate of 10 ^{0}C/min under nitrogen purge [11].

3.2.3. Attenuated Total Reflection – Fourier Transform Infra-red Spectroscopy (ATR-FTIR)

Infrared spectra were recorded on a PerkinElmer Spectrum 1 FT-IR Spectrometer equipped with a UATR and a diamond/ZnSe crystal accessory. Each spectrum was scanned in the range of 650–4000 cm^{-1} with a resolution of 4 cm^{-1} and a minimum of six scans were collected and averaged in order to gain good quality spectra. Data were evaluated using Spectrum v 5.0.1. software.

3.2.4. Solid state Nuclear Magnetic Resonance (ssNMR) spectroscopy

All measurements were performed using a broadband 3.2 mm solid state NMR probe and a 400 MHz JEOL ECX400 spectrometer. Samples were prepared by packing an adequate amount of each sample, as received, into 3.2 mm Silicon nitride (Si3N4) solid state NMR rotors. The sample spinning rate was set to 10 kHz. ^{13}C NMR spectra (100 scans) were recorded using the CPMAS (Cross Polarisation – Magic Angle Spinning) pulse sequence. Prior to each spectrum, the corresponding T_1 constant (spin-lattice relaxation) was measured using the saturation recovery pulse sequence.

3.3 Elemental analysis

Elemental analysis was carried out using an Exeter Analytical CE440 CHN analyser. The molar amount of carbon as carbon dioxide, nitrogen, as nitrogen oxide and hydrogen as water, was determined by oxidation of the sample (n=3, around 10 mg) and the thermal conductivity analysis of obtained gases and water vapour.

3.4. Cocrystal structural determination

Powder X-ray diffraction for structure determination

X-ray powder diffraction patterns were recorded at room temperature on a Bruker D8 ADVANCE high-resolution laboratory X-ray powder diffractometer using Cu-Kα1 radiation from a primary Ge(111)-Johansson-type monochromator and a Våntec position-sensitive

detector (PSD) in Debye-Scherrer geometry. Data collection spanned over 20 hours, covering a range of 2° to 65° along 2θ in steps of 0.008° with a 6° opening of the PSD. The sample (crystals obtained by crystallization from solution, see 3.1.3.) was spun during measurement to ensure better particle statistics. Structure determination and refinement of powder data were carried out using the program TOPAS 4.1 [12] and DASH 4.2 [13]. Indexing was carried out via the singular value decomposition method as implemented within TOPAS [14]. Confirmation by Rietveld refinement of the solved structure was performed [15]. The peak profile and precise lattice parameters were determined by Le Bail fits [16] using the fundamental parameter (FP) approach of TOPAS [17], allowing for the determination of microstructural properties such as domain size and microstrain. For the modelling of the background, fourth-order Chebychev polynomials were employed. The crystal structure was solved by the global optimization method of simulated annealing (SA) in real space as implemented by DASH [13]. The relative positions of the molecules were not known a priori, thus two independent molecular models were used using standard bond lengths and angles. Slack bond length, bond angle and planarity restraints were introduced to stabilise the subsequent Rietveld refinement [15]. For the final Rietveld refinement, all profile and lattice parameters were released and all atomic positions were subjected to refinement using soft bond and angle constraints. The program Mercury 2.3 was used for illustrating the molecular structures [10].

3.5. Solubility studies

3.5.1. Equilibrium/Apparent solubility

The solubility (in water at 37 °C) was determined using a 24-hour (for SD) and 1-hour (for 4-ASA) shake flask method [18]. The equilibration time in the case of 4-ASA was selected based on previously reported work by Forbes et al. (1995) which showed that, due to degradation of 4-ASA in solution, an equilibration time of 1 hour is appropriate to measure its apparent solubility [19]. The study was performed in triplicate.

3.5.2. Phase-solubility studies

In order to examine complexation between the compounds, excess (approximately 2-3 times the amount expected to achieve saturation solubility) of solid SD was added to 10 ml aqueous solution aliquots containing different concentrations (0.00065 – 0.02 M) of 4-ASA in glass ampoules, which were heat sealed. The ampoules were placed horizontally in a thermostated

waterbath at 37 °C and shaken at 100 cpm for 1 hour. The supernatant was filtered using 0.45 μm membrane filters (PVDF - Cronus®) and analysed for sample concentration by HPLC. The remaining solid phase was characterised by PXRD. The study was performed in triplicate.

3.5.3. Transition concentration (Ctr) measurement

The cocrystal transition concentration (Ctr) was determined as previously described [20]. The experiments were performed in triplicate.

3.5.4. pH-dependent solubility

The cocrystal solubility was determined at different pH values by the addition of small volumes of 1M HCL and 1M NaOH using the shake-flask method. Solid phases and solution concentrations were analysed after 1 hour equilibration and the pH was measured. The solid was characterised by PXRD and the concentration of the supernatant was analysed by HPLC after filtration through 0.45 μm membrane filters (PVDF - Cronus®). The experiments were performed in triplicate.

3.5.5. Dynamic solubility studies

Dynamic solubilities were determined in a jacketed glass vessel (50 ml) connected to a pump and a waterbath, sitting on a magnetic stirrer. Excess amount of solid was added to 30 ml of water and the solution was stirred at a temperature of 37 °C for up to 1 hour. Samples of 2 ml were withdrawn at appropriate intervals, filtered through 0.45 μm membrane filters (PVDF - Cronus®) and analysed for sample content by HPLC. At each time point an aliquot of the solid phase was withdrawn, dried at ambient temperature and examined by PXRD. The experiments were performed in triplicate.

3.6. Intrinsic dissolution studies

The intrinsic dissolution rate (IDR) of solid materials was determined using constant surface area discs as previously described [21]. The stationary disc method was used in preference to the rotating disc method (Wood's apparatus) as the latter is less suited to multi-component systems, with a greater tendency for disintegration and thus disruption of the constant surface area, than with the stationary disc method [22]. The IDR was determined from the slope of the dissolution time profiles. Initial and limiting rates were determined within the first 10 min and

between 10 and 60 min, respectively. The discs were recovered, dried at ambient temperatures and then analysed by PXRD and FTIR for surface changes.

3.7. High Performance Liquid Chromatography (HPLC)

Concentrations of SD and 4-ASA in solutions were determined using a Shimadzu HPLC Class VP series with a LC-10AT VP pump, SIL-10AD VP autosampler and SCL-10VP system controller. The mobile phase was vacuum filtered through a 0.45 μm membrane filter (Gelman Supor-450). Separation was performed on a Phenomenex Inertsil ODS (3) C18 column (150 mm length, diameter 4.6 mm, particle size 5 μm) at a UV detection wavelength of 260 nm with an injection volume of 10 μL. The mobile phase consisted of methanol/buffer pH 6.5 40/60 (v/v). The buffer was prepared from a 50 mM potassium hydrogen phosphate solution adjusted to pH 6.5 with 100 mM phosphoric acid. The elution was carried out isocratically at ambient temperature with a flow rate of 1 ml/min. Class-VP 6.10 software was used for peak evaluation. The calibration curves were linear for both components between 0.5 μg/ml and 100 μg/ml (R^2 > 0.998). For SD the calculated limit of detection (LOD) was 0.6 μg/ml and the limit of quantification (LOQ) was 1.8 μg/ml. For 4-ASA the LOD was 1.3 μg/ml and the LOQ was 4.2 μg/ml.

3.8. Dynamic Vapor Sorption (DVS)

Vapour sorption experiments were carried out on a DVS Advantage-1 automated gravimetric vapour sorption analyser (Surface Measurement Systems Ltd., London, UK). The temperature was maintained constant at 25.0 ± 0.1 °C. Powder (10 mg) was loaded into the system. The sample was analysed from 0% to 90% relative humidity (RH) in 10% steps and the same for desorption. The sample was equilibrated at each of RH conditions until constant mass (dm/dt ≤ 0.002 mg/min) was reached. The reference sample mass (m_0) for each experiment was recorded at 0% RH. The RH isotherms were calculated from the complete sorption and desorption profiles. The solid phase after sorption and desorption was characterised by PXRD for solid state changes. The experiment was performed in triplicate.

3.9. Long-term stability test

Solid state stability of the bulk material was carried out using an Amebis Test System (Amebis, Ireland) under conditions of 60 ± 5% RH at 25 ± 5 °C. The samples were placed in Amebis humidity devices at 60% RH and stored in an oven at 25 °C. The test conditions were monitored using the Amebis Control Software. Samples were assayed in duplicate after 1, 2, 6 and 12 months using PXRD, DSC, FTIR and HPLC.

3.10. Statistical analysis

3.10.1. Two sample t-test

Microsoft® Excel data analysis software was used to determine statistical significance. The two sample t-test was used to compare the means and standard deviations of two independent samples at a significance level of $\alpha=0.05$.

3.10.2. ANOVA

Origin Lab® data analysis software was used to determine statistical significance using one-way ANOVA at a significance level of $\alpha=0.05$.

3.10.3. Linear regression

Linear regression analysis was performed using the method of least squares by Microsoft® Excel software. The adequacy of the fit was assessed from the regression coefficient (R^2).

4. Results and discussion

4.1. Polymorphic SD:4-ASA cocrystal: solid state properties

4.1.1. Milled SD:4-ASA

Powder X-Ray Diffraction

PXRD analysis revealed that products obtained by dry milling displayed diffraction patterns with peaks at the same positions regardless of the ratio in the mixture and all diffraction peaks could be superimposed with those of the single compounds. Furthermore, the intensity of the diffraction peaks decreased with increasing milling time which was attributed to amorphisation induced by milling (Figure 1A). In contrast, the liquid-assisted milled products showed patterns with characteristic diffraction peaks, which differed from those of the single components (Figure 1B). However, the mixture ratios of SD:4-ASA 1:2 (Figure 1S-B g–i, supporting information) and 2:1 (Figure 1S-B a–c, supporting information) showed additional

diffraction peaks which superimposed with those of 4-ASA raw material and/or SD raw material, respectively. The milling time was not found to have an influence on the PXRD patterns.

Thermal Analysis

Results of thermal analysis of the dry milled SD:4-ASA products are shown in Figure 1C and Table 1S (see supporting information). As the content of SD increased in the mixture, the endothermic melting event shifted towards the melting temperature of SD (T_m = 197.16 ± 0.43 °C, ΔH_f = 130.45 ± 6.60 J/g). Melting of all dry milled products was associated with a significant mass loss and thus with degradation (Figure 2S, supporting information). The 1:1 mixtures showed a single melting event (Figure 1C), while the non-equimolar mixtures revealed, as in the case of the 1:2 ratio, a double peak endotherm shifted towards the melting temperature of 4-ASA (T_m = 139.07 ± 0.93 °C, ΔH_f = 392.80 ± 7.33 J/g) (Figure 1S-C g–i, supporting information) and in the case of the 2:1 ratio a second, small melting event attributed to SD was observed (Figure 1S-C a–c, supporting information). From these results it was concluded that, in contrast to the 1:1 product, the non-equimolar mixtures contained excess amount of either SD or 4-ASA raw material. For all dry milled products, regardless of the mixture ratio, an exotherm in the temperature range between 65 and 95 °C, which increased in enthalpy with increasing milling time, was observed (Figure 1C and Figure 1S-C, supporting information) and was not associated with a significant mass loss by TGA. This was attributed to crystallisation of an amorphous content induced by milling [23,24]. DSC analysis of the single components when milled separately under the same conditions showed, in the case of SD, a similar exothermic event prior to melting as for the co-milled systems whereas 4-ASA remained crystalline at the given milling conditions (Figure 3S, supporting information). For the liquid-assisted milled products, it was found that, similar to the dry milled products, an increasing amount of SD in the mixture resulted in a shift of the endothermic melting event towards the melting temperature of SD (Figure 1S-D, supporting information). Only the 1:1 mixtures showed a single melting event (Figure 1D and Table 1S supporting information), while the non-equimolar mixtures revealed a double peak endotherm, as for the dry milled materials (Figure 1S-D, supporting information). The thermograms did not show any evidence of amorphisation since no exothermic events prior to melting were observed (Figure 1D). All products melted with decomposition (Figure 4S, supporting information).

4.1.2. Spray-dried SD:4-ASA

Powder X-Ray Diffraction

PXRD patterns of the spray-dried products are shown in Figure 2A. All three spray-dried products differed from each other and from the single components as well as from the dry and liquid-assisted milled products. Spray drying from a 2:1 component mixture resulted in a product that showed a broad halo, characteristic of the amorphous state, with some diffraction peaks with very low intensity (Figure 5S-A a, supporting information). The products of the SD:4-ASA 1:1 (Figure 2A a) and 1:2 ratio (Figure 5S-A c, supporting information) showed similar diffraction patterns, whereas the 1:2 product revealed some additional diffraction peaks at around 26 and 27 degree 2θ which can be attributed to 4-ASA.

Thermal Analysis

Results of thermal analysis of the spray-dried SD:4-ASA products are shown in Figure 2B and Table 1S (see supporting information). For the SD:4-ASA 2:1 spray-dried product (Figure 5S-B a, supporting information) a glass transition (Tg) at 68.46 ± 0.20 °C, characteristic of the amorphous state and thus consistent with the PXRD data (Figure 5S-A a, supporting information), followed by two exothermic crystallisation events, corresponding to crystallisation of the amorphous phase, and then a endothermic melt event, were observed. The amorphous phase may be attributed to partially amorphous SD induced by spray drying, as it has been found that when the components were spray-dried separately under the same conditions: SD showed an exothermic event in the same temperature range as observed for the SD:4-ASA 2:1 spray-dried product prior to melting, while 4-ASA revealed a melting event only and remained crystalline (Figure 6S, supporting information). In contrast, co-spray drying from a 1:1 ratio revealed a product with a single melting peak (Figure 2B a) occurring at the same temperature as the melting peak of the 1:1 liquid-assisted milled material (Figure 2B c). Melting of each product was found to be associated with decomposition, as evidenced by TGA analysis (Figure 7S, supporting information). In the case of the co-spray-dried materials, the product of the 1:2 SD:4-ASA ratio (Figure 5S-B c, supporting information) showed a broad asymmetric melting event shifted towards the melting temperature of 4-ASA (T_m = 139.07 ± 0.93 °C), similar to the 1:2 SD:4-ASA dry milled and liquid-assisted milled products, indicative of excess amount of 4-ASA.

Based on the above results, it was concluded that SD and 4-ASA formed only 1:1 cocrystals. Cocrystals of other stoichiometries (1:2 and 2:1) were not observed. The use of dry milling of SD with 4-ASA as coformer did not result in cocrystal formation, while this method has been reported as successful in cocrystal formation for structurally related aromatic carboxylic acids, such as benzoic and salicylic acid coformers [25]. Although dry milling did not result in cocrystal formation, this may be a result of insufficient mechanical force that has been provided under the given experimental conditions. Instead, binary crystalline mixtures with some amorphous phase, which increased with increasing milling time, were obtained. Similar findings which showed that amorphisation is a function of milling time have been reported by other authors [23,24].

Liquid-assisted milling using ethanol as solvent resulted in the formation of the SD:4-ASA 1:1 form I cocrystal (previously reported by Caira in 1992 [9]). None of the liquid-assisted milled products showed evidence of amorphisation. In contrast to dry milling, these findings demonstrate the effectiveness of the liquid-assisted milling method in producing cocrystals, which has been previously reported by several authors [26,27].

By spray drying from a solution containing a 1;1 molar ratio of the two components, an apparently different form of the SD:4-ASA 1:1 cocrystal was prepared. All further solid state characterisation was focused on the SD:4-ASA 1:1 liquid-assisted milled (form I) and spray-dried products (form II).

4.2. Elemental Analysis

Characterisation by elemental analysis of the carbon, hydrogen and nitrogen composition of the liquid-assisted milled and spray-dried product is shown in Table 1. For both products the same elemental composition was detected and showed consistency with the known cocrystal molecular formula, $C_{12}H_{14}N_4O_2S$.

4.3. ATR-FTIR

Results of IR spectroscopy are illustrated in Figure 3A. Distinctive bands in the higher frequency range were observed for the single components. SD showed three characteristic bands: two bands at around 3441 cm^{-1} and 3338 cm^{-1} attributed to the asymmetric and symmetric NH_2 stretching bands of the amine group respectively and one stretching band at approximately 3235 cm^{-1} attributed to the sulfonamide or amidine NH group (Figure 3A d). 4-ASA displayed two characteristic bands at around 3493 cm^{-1} and 3386 cm^{-1} referring to the

asymmetric and symmetric NH_2 stretching bands of the amine group respectively (Figure 3A c). The SD:4-ASA 1:1 liquid-assisted milled product (form I) (Figure 3A b) showed bands at 3468, 3415, 3369 and 3339 cm^{-1} corresponding to the NH_2 stretching vibrations of the amine groups and shifts to different wavenumbers with respect to the pure components (Figure 3A c and d). A shift of the band corresponding to the OH bending of the carboxylic acid group in 4-ASA merging with the band attributed to the sulfone (SO_2) group in SD (at 1300 cm^{-1}) was found at 1274 cm^{-1} (Figure 3A b). The observed shifts are indicative of molecular interactions such as hydrogen bonding. The spray-dried material (form II) showed different peaks compared to the liquid-assisted milled product. As shown in Figure 3A a, the bands at 3482 cm^{-1} and at 3372 cm^{-1} are attributable to the NH_2 stretching bands of the amine groups which are also shifted towards other wavenumbers and are therefore attributable to intermolecular interactions which differed to those of the single components and liquid-assisted milled product. Further differences between both materials were observed by shifts of bands corresponding to the sulfone (SO_2) stretching vibrations in SD and to the carboxyl group (OH bending) in 4-ASA at 1315 and 1275 cm^{-1}, respectively.

4.4. ssNMR

To elucidate the structural differences between the SD:4-ASA 1:1 liquid-assisted milled and spray-dried product, solid state NMR analysis was performed. The ^{13}C CPMAS spectra are shown in Figure 3B and peak assignments are presented in Table 2. Both SD and 4-ASA revealed sharp and narrow signals indicative of highly ordered (crystalline) structures (Figure 3B c and d). The relaxation time constants (T_1) were found to be 48 seconds and 220 seconds for SD and 4-ASA, respectively. Generally, highly ordered, crystalline samples tend to have long relaxation times and thus high T_1 due to the long distances between individual nuclei in crystals. On the other hand, short relaxation times corresponding to low T_1 values are usually observed for amorphous materials due to the proximity of each nucleus to surrounding nuclei [28].

For the liquid-assisted milled product (form I) (Figure 3B b), the T_1 constant was 16 seconds and therefore significantly lower than the corresponding values for the single components, indicating that the product is less ordered than SD and 4-ASA raw materials. The peaks were sharp and narrow. Most signals have shifted towards higher or lower ppm numbers with respect to the single components. For the SD:4-ASA 1:1 spray-dried product (form II) (Figure 3B a), a T_1 of 7.5 seconds was found. This value was lower than the values for the liquid-

assisted milled sample and the single components and indicates that the spray-dried product is less ordered in nature, which is supported by the broader peaks found in the spectrum. The characteristic shifts observed in the spectrum, differed to those of the liquid-assisted milled sample and were indicative of molecular interactions between the components.

A physical mixture of SD and 4-ASA in 1:1 molar ratio and SD and 4-ASA after being spray-dried separately was also analysed (Figure 8S, supporting information). For the physical mixture, the T_1 value was 65 seconds and all peaks in the spectrum were superimposed with those of SD and 4-ASA, indicating that simply mixing of the two components did not alter the chemical structure. Spray-dried SD and 4-ASA showed T_1 values of 12.5 and 19.5 seconds, respectively and displayed broader peaks when compared to unprocessed materials. The T_1 values were significantly lower than the unprocessed materials, indicating that the components became more disordered on spray drying. The peak broadening of the single components was not found to be attributable to the peak broadening of the SD:4-ASA co-spray-dried material (form II). Therefore, it can be concluded that the broader peaks obtained from co-spray drying associated with shifts are not only a result of a more disordered state, but confirm that the carbon atoms are chemically different to those of the liquid-assisted milled product, a physical mixture and the single components.

In summary, analyses using FTIR and ssNMR further confirmed the solid state difference between the SD:4-ASA 1:1 liquid-assisted milled and spray-dried form. While liquid-assisted milling of SD and 4-ASA in 1:1 ratio resulted in the formation of the same cocrystal as reported by Caira (1992) [9] (form I), the spray-dried product revealed noticeable differences which are attributed to differences in both molecular interactions between SD and 4-ASA and solid state nature, indicating that a polymorphic form of the SD:4-ASA 1:1 cocrystal (form II) has been generated by spray drying.

4.5. Cocrystal structural determination

For determination of the crystal structure using single crystal X-ray diffraction (SC-XRD), single crystals of the form II cocrystal were grown from ethanol and acetone by solvent evaporation as described in section 3.1.3. Characterisation of the obtained crystals by PXRD and DSC confirmed consistency with the spray-dried product (data not shown). However, due to observed non-crystallographic reflections, the structure could not be immediately solved.

Alternatively, the PXRD technique was used to determine the crystal structure, which has been reported to be a successful tool when single crystal data cannot be obtained [29]. It was found that the form II cocrystal had an orthorhombic unit cell with $P2_12_12_1$ space group, whereas the form I cocrystal was reported to exist in a triclinic unit cell with space group P-1 [9]. A summary of the crystallographic data is presented in Table 3 and full lists of atomic coordinates, together with intramolecular distances and angles, can be found in the supporting information (Tables 2S–6S).

Intermolecular interactions in the form I cocrystal show hydrogen-bond preferences of O-H….N and N-H....O between the amidine moiety of SD and the acid group of 4-ASA (Figure 4A). In the form II cocrystal interactions were found between C-H….N and C-H....O involving the amidine and sulfoxy group of SD and the aromatic hydrogens of 4-ASA (Figure 4B). In the form II cocrystal there are rather strong (pi stacking) H bonds between an O on the sulfadimidine molecule and the aromatic ring of a neighbouring 4-aminosalicylic acid molecule (2.85 Å and 3.10 Å). There are also strong H bonds present between the carboxylate and alcohol groups on neighbouring salicylic acid molecules (1.9 Å and 2.4 Å respectively), and H bonds between neighbouring sulfadimidine molecules (3.00 Å). Such bonding between like molecules is unusual, however, there are examples in the literature where the interactions between carboxylic acid and alcohol groups on neighbouring molecules of the same compound are preferred over interactions with the coformer that usually emerge in the form of R2,2(8) graph sets involving carboxylate, amine and amido moieties [30,31]. The SD molecules in the new form II cocrystal adopt a cage-like arrangement, with 4-ASA molecules aligned diagonally across the cavity (Figure 4D).

The unit cell volume of the form II was found to be almost double of that of the form I cocrystal, possibly due to a difference in molecular packing flexibility, thus posing torsional restrictions. In the form I cocrystal, the 4-ASA and the dimethylpyrimidine portion of SD are essentially coplanar, forming sheets with an interlayer distance of 3.409 Å (Figure 4C). The molecules in Form II do not show pi stacking between the aromatic group of the sulfadimidine and the aromatic ring of the amino salicylic acid, and this leads to a longer unit cell length in the *a* direction, which in turn translates into a larger unit cell volume.

4.6. Solubility studies

The equilibrium and apparent solubility of SD and 4-ASA were found to be 2.30 x 10^{-3} ± 1.91 x 10^{-5} mmol/ml and 1.49 x 10^{-2} ± 4.75 x 10^{-6} mmol/ml, respectively. As demonstrated by

Good and Rodríguez-Hornedo (2009) [20], cocrystal solubility can be estimated through only a single measurement from the transition concentration at which the cocrystal and drug are in equilibrium with the solution. A good estimation of the cocrystal solubility based on C_{tr} measurements requires that solution complexation does not play a role [20]. To determine whether solution complexation was present, phase-solubility studies were performed. As shown in Figure 5A, increasing 4-ASA concentrations in solution did not have an impact on the concentration of SD in solution. The measured SD concentration for solutions which contained ≥ 0.0026 mmol/ml 4-ASA did not change significantly and was $2.45 \times 10^{-3} \pm 3.0 \times 10^{-5}$ mmol/ml. When compared to S_0 (SD concentration in the absence of 4-ASA, $S_0 = 2.30 \times 10^{-3} \pm 1.91 \times 10^{-5}$ mmol/ml), the measured increase and thus solution complexation of SD in the presence of 4-ASA was considered to be negligible.

The prediction of cocrystal solubility dependence on pH has been previously described for different components by Bethune et al., 2009 [32]. However, no model has been reported for a cocrystal containing two amphoteric components. Therefore, for the SD:4ASA 1:1 cocrystal a new theoretical model based on the equilibrium reactions for cocrystal dissociation and ionisation has been established from which the pH-dependent cocrystal solubility was predicted by the following equation:

$$S_{cocrystal} = \sqrt{K_{sp}\left(1 + \frac{[H^+]}{K_{a1,SD}} + \frac{K_{a2,SD}}{[H^+]}\right)\left(1 + \frac{[H^+]}{K_{a1,4ASA}} + \frac{K_{a2,4ASA}}{[H^+]}\right)} \qquad \text{(Eq.1)}$$

where K_{sp} is the solubility product and K_{a1} and K_{a2} are the acid ionisation constants for SD (drug) and 4-ASA (coformer), respectively. The model is described in detail in the supporting information.

Based on the measured C_{tr}, the pH and the known acid constants for the SD ($K_a = 2.79$ and 7.4) and the 4-ASA ($K_a = 2$ and 3.56), a K_{sp} of $1.91 \times 10^{-6} \pm 1.57 \times 10^{-7}$ M^2 was calculated using the following equation:

$$K_{sp} = \frac{[SD]_{tr}\,[4ASA]_{tr}}{\left(1 + \frac{[H^+]}{K_{a1,SD}} + \frac{K_{a2,SD}}{[H^+]}\right)\left(1 + \frac{[H^+]}{K_{a1,4ASA}} + \frac{K_{a2,4ASA}}{[H^+]}\right)} \qquad \text{(Eq. 2)}$$

The obtained K_{sp} allowed further prediction of the cocrystal solubility for other pH values using Equation 1. Figure 5B shows the resulting cocrystal solubility profile, dependent on the pH. For the single components the pH-dependent solubility was derived from the Henderson-Hasselbalch relationship. The SD:4-ASA 1:1 form I cocrystal was less soluble than its single components in the acidic region at pH < 4 and became more soluble than SD at pH > 4. Experimentally measured solubilities of the cocrystal at other pH values (2.3 and 3.76) were found to be in good agreement with the predictions and were determined according to the following equation for a 1:1 cocrystal referring to Nehm et al., (2006)[33]:

$$S_{cocrystal} = \sqrt{[drug][coformer]}$$ (Eq. 3)

PXRD analysis of the solid phases at equilibrium confirmed the presence of cocrystal as a single phase and thus its stability at the given pH. In contrast, at pH = 6.8 the measured concentration was found to be lower than the predicted solubility (Figure 5B). PXRD analysis of the solid phase detected a mixed phase of cocrystal and SD attributed to the presence of the diffraction peak at 9.35° 2θ (Figure 5C a). At pH = 6.8 the cocrystal was unstable by transforming to SD and explained the deviation of the experimentally determined solubility from the predicted profile (Figure 5B).

For determination of the solubility of the SD:4-ASA 1:1 form II cocrystal, initial solubility experiments using the shake-flask method were performed. However, after 1 hour equilibration time, the solid phase had fully converted to the form I cocrystal and SD (verified by PXRD, data not shown). For more detailed information, dynamic solubility studies were performed. After only 30 seconds, the form II cocrystal converted, to some extent, to the form I cocrystal attributed to the presence of the diffraction peak at 10.25° 2θ (Figure 5D a). At 10 minutes, a third phase was detected in the solid residue, corresponding to SD as shown by the characteristic diffraction peak at 9.35° 2θ (Figure 5D b). At 20 minutes almost all diffraction peaks attributed to the form II cocrystal had disappeared (Figure 5D c) and at 60 minutes form II had fully converted to form I cocrystal and SD (Figure 5D d).

The concentration-time profile of the form II cocrystal revealed that the concentrations of SD and 4-ASA were non-equimolar. SD exhibited a significantly higher concentration at earlier

time points (peak at 8 minutes) followed by a decrease after 10 minutes with the trend to level out with the 4-ASA concentration with increasing time (Figure 9S, supporting information). The decrease was explained by the phase transformation, as was shown by PXRD analysis. In contrast to form II, the form I cocrystal showed equimolar solution concentrations of SD and 4-ASA (Figure 10S, supporting information) which were stable over 60 minutes, as confirmed by PXRD analysis of the solid residue at each time point (data not shown).

These results indicated that the SD:4-ASA 1:1 form II cocrystal forms an unstable, supersaturated solution which undergoes a rapid solution-mediated transformation into the more stable form I associated with precipitation of SD. Considering the given conditions, it was not possible to determine the solubility of form II. The non-equimolar concentrations in solution at early timepoints in the dynamic solubility studies reflect the dynamic and simultaneous effects of dissolution, conversion and precipitation from solution.

4.7. Intrinsic dissolution studies

The intrinsic dissolution profiles of the pure components are shown in Figure 6A. The dissolution of both components was linear over time ($R^2 > 0.97$), whereas 4-ASA dissolved around nine times faster than SD. Analysis of the compact surface at the end of the study by IR and PXRD (data not shown) verified that no phase changes occurred. The SD:4-ASA 1:1 form I cocrystal showed linear ($R^2 > 0.99$), non-equimolar release with a ratio of 1:1.3 of SD:4-ASA at each time point (Figure 6B). No changes of the surface composition were detected, as confirmed by IR and PXRD analysis (data not shown). SD exhibited a 1.4-fold higher and 4-ASA a 5-fold lower dissolution rate compared to the pure components. In the case of SD:4-ASA 1:1 form II cocrystal, the dissolution was initially measured from 10 – 60 minutes. However, at the end of the study the surface composition revealed changes. PXRD revealed the presence of diffraction peaks at 9.35 and 10.25° 2θ, characteristic of SD and the form I cocrystal, respectively. These results confirmed that the form II cocrystal transformed to form I and SD during dissolution. Further studies were therefore performed for lower time points (2–10 minutes). The dissolution of both components was linear ($R^2 > 0.98$) and nearly equimolar (1:0.9 SD:4-ASA) over time. For SD, the dissolution rate was around 1.7-fold and 1.2-fold higher compared to pure SD and the form I cocrystal, respectively, while 4-ASA showed a more than 6-fold and approximately 1.2-fold lower dissolution than pure 4-ASA and the form I cocrystal, respectively (Figure 6C). No phase changes at the surface of the compact were detected, as confirmed by IR and PXRD analysis (data not shown).

For comparison, the dissolution behaviour of a physical equimolar mixture of SD and 4-ASA was studied (Figure 6D). Both components showed linear profiles ($R^2 > 0.99$), although 4-ASA dissolved initially faster, followed by a slower linear release. The dissolution rate of SD from the physical mixture did not differ significantly to pure SD, but was 1.3-fold and 1.5-fold lower than from the form I and form II cocrystal, respectively. At the end of the study the surface composition revealed changes. PXRD confirmed the presence of the form I cocrystal attributed to the characteristic diffraction peaks at 10.25 and 13.75° 2θ (data not shown).

4.8. Dynamic vapour sorption

The dynamic vapour sorption and desorption isotherms of the form I and form II cocrystal are illustrated in Figure 7A. In comparison to the form II cocrystal, the form I cocrystal sorbed less water over the entire humidity range. The maximum water sorption of the form I cocrystal was below 0.3%, where most water was sorbed between 70 and 90%. The desorption behaviour was similar with a slight hysteresis effect in the humidity range of 90 to 40% RH, followed by merging with the sorption profile below 40% RH. In contrast, the form II cocrystal showed a maximum water sorption below 1% and a relatively strong increase in water sorption between 70 and 90% RH. The desorption behaviour was similar and associated with a small hysteresis effect over the entire humidity range. The cocrystals can be classified as slightly hygroscopic according to the hygroscopicity classification system[34]. As was shown by solid state NMR, the form I cocrystal was more ordered (crystalline), whereas the form II cocrystal showed a less ordered crystalline behaviour. Amorphous materials tend to sorb more water vapour than crystalline materials, which would explain the DVS results of the form II cocrystal relative to form I.

PXRD analysis of the materials recovered at the end of the experiment (0% RH) and at 90% RH revealed no changes compared to the starting materials (Figure 7B), which confirmed that both cocrystal forms remained unchanged under DVS experimental conditions.

4.9. Long-term stability test

The form I and form II cocrystals did not undergo changes over 12 month storage under conditions of 60% RH at 25 °C. This was confirmed by PXRD analysis, which showed that the diffraction patterns remained unchanged over the entire time for both, the form I (Figure 7C) and the form II cocrystal (Figure 7D). Further characterisation by DSC and IR

spectroscopy was consistent with the results from PXRD and no substantial changes occurred over 12 months at the given storage conditions. Moreover, HPLC analysis revealed that both materials did not undergo chemical changes during the stability study. The SD:4-ASA molar ratio of both the form I and form II cocrystals remained constant over time (data not shown).

5. Conclusions

SD:4-ASA 1:1 cocrystals can be generated by liquid-assisted milling and spray drying, while this was not possible using dry milling under the experimental conditions used. Cocrystals of other stoichiometries (1:2 and 2:1) have not been observed. By liquid-assisted milling the SD:4-ASA 1:1 form I cocrystal was formed. By spray drying a polymorphic form (form II) of the SD:4-ASA 1:1 cocrystal was discovered which could also be obtained by solvent evaporation from ethanol and acetone. The crystal structure of the SD:4-ASA 1:1 form II polymorph was derived from powder diffraction data. The solubility of the SD:4-ASA 1:1 cocrystal was dependent on the pH and could be predicted by a model established for a two amphoteric component cocrystal. The form I cocrystal was found to be thermodynamically more stable in aqueous solution than form II, which showed transformation to form I. Dissolution studies revealed that the dissolution rate of the poorly water soluble SD from both cocrystal forms was enhanced when compared to a physical equimolar mixture and pure SD. The dissolution rates were consistent with the corresponding solubilities. Both cocrystal forms were slightly hygroscopic and stable on a long-term storage.

Figure captions

Figure 1. PXRD patterns and DSC thermograms of SD and 4-ASA, dry and liquid assisted-milled in 1:1 molar ratio. A) PXRD patterns of SD and 4-ASA dry milled; B) PXRD patterns of SD and 4-ASA liquid-assisted milled using ethanol; C) DSC thermograms of SD and 4-ASA dry milled and D) DSC thermograms of SD and 4-ASA liquid-assisted milled using ethanol. Key: (a) SD:4-ASA 1:1 milled 45 min, (b) SD:4-ASA 1:1 milled 30 min, (c) SD:4-ASA 1:1 milled 15 min, (d) 4-ASA, raw material (e) SD, raw material.

Figure 2. PXRD patterns and DSC thermograms of spray-dried SD and 4-ASA systems in 1:1 molar ratio. A) PXRD patterns and B) DSC thermograms. Key: a) SD:4-ASA 1:1 spray-dried, b) SD:4-ASA 1:1 dry milled 15 min, c) SD:4-ASA 1:1 liquid-assisted milled 15 min, d) 4-ASA, raw material and e) SD, raw material.

Figure 3. FTIR and ^{13}C CPMAS spectra. A) FTIR spectra and B) ^{13}C CPMAS spectra . Key: a) SD:4-ASA 1:1 spray-dried product, b) SD:4-ASA 1:1 liquid-assisted milled product, c) 4-ASA, raw material and d) SD, raw material. The signals labelled by the asterisks indicate spinning side bands.

Figure 4. Crystal structure and molecular interactions between SD and 4-ASA. A) Molecular interactions of the SD:4-ASA 1:1 cocrystal proposed by Caira (1992) [9], B) Molecular interactions in the SD:4-ASA 1:1 form II cocrystal calculated from PXRD data, C) Crystal structure of SD:4-ASA 1:1 form I cocrystal (determined from single crystal data by Caira [9]) viewed along the *b* axis and D) crystal structure of SD:4-ASA 1:1 form II cocrystal (calculated from PXRD data) viewed along the *a* axis; Key: dotted black lines indicate hydrogen bonds and the numbers represent the corresponding bond length.

Figure 5. Solubility studies and PXRD patterns. A) Phase-solubility profile of SD (mmol/ml) as a function of 4-ASA concentration. S_0 is the equilibrium solubility of SD in the absence of 4-ASA; B) Theoretical pH solubility profile (37 °C) for the SD:4-ASA 1:1 form I cocrystal containing two amphoteric components. The solid line represents the cocrystal solubility, the dashed and dotted lines show the theoretical SD and 4-ASA solubility dependent on the pH (derived from the Henderson-Hasselbalch relationship) and the cross symbols are experimentally obtained solubility data for the cocrystal; C) PXRD patterns of SD:4-ASA 1:1 form I cocrystal phases at different solution pH compared to the cocrystal before the study

and the single components: a) cocrystal at pH = 6.8, b) cocrystal at pH = 3.76, c) cocrystal at pH = 2.30, d) form I cocrystal before subjected to solubility test, e) 4-ASA, raw material and f) SD, raw material and D) PXRD patterns of the solid phase during dynamic solubility studies performed in water (37 °C) of the SD:4-ASA 1:1 form II cocrystal: a) at 30 seconds, b) at 10 minutes, c) at 20 minutes, d) at 60 minutes compared to e) SD:4-ASA 1:1 form II before subjected to solubility test, f) SD:4-ASA 1:1 form I cocrystal before subjected to solubility test and g) SD, raw material.

Figure 6. Dissolution profiles obtained in water at 37 °C. A) SD and 4-ASA; B) SD:4-ASA 1:1 form I cocrystal; C) SD:4-ASA 1:1 form II cocrystal and D) SD:4-ASA 1:1 physical mixture. The dashed line refers to the initial rate of 4-ASA. Key: Diamonds symbolise SD, triangles represent 4-ASA.

Figure 7. Stability studies. A) Moisture sorption and desorption profiles of SD:4-ASA 1:1 form I (closed and open triangles) and form II (closed and open diamonds) cocrystal at 25 °C; B) PXRD patterns before and after DVS experiments: a) SD:4-ASA 1:1 form II cocrystal, recovered after DVS at 90% RH, b) SD:4-ASA 1:1 form II cocrystal, recovered after DVS at 0% RH, c) SD:4-ASA 1:1 form II cocrystal, before DVS study, d) SD:4-ASA 1:1 form I cocrystal, recovered after DVS at 0% RH and e) SD:4-ASA 1:1 form I cocrystal, before DVS study; C) PXRD patterns of the SD:4-ASA 1:1 form I cocrystal analysed at different time points during long-term stability test: a) before the study; b) 1 month; c) 2 months; d) 6 months and e) 12 months and D) PXRD patterns of the SD:4-ASA 1:1 form II corystal analysed at different time points during long-term stability test: a) before the study; b) 1 month; c) 2 months; d) 6 months and e) 12 months.

References

1. Serrano Lopez DR, Lalatsa A. 2013. Peptide pills for brain diseases? Reality and future perspectives. Therapeutic delivery 4(4):479–501.

2. Babu NJ, Nangia A. 2011. Solubility Advantage of Amorphous Drugs and Pharmaceutical Cocrystals. Cryst Growth Des 11(2662–2679).

3. Vishweshwar P, McMahon JA, Bis JA, Zaworotko MJ. 2006. Pharmaceutical co-crystals. Journal of pharmaceutical sciences 95(3):499–516.

4. Blagden N, de Matas M, Gavan PT, York P. 2007. Crystal engineering of active pharmaceutical ingredients to improve solubility and dissolution rates. Advanced drug delivery reviews 59(7):617–630.

5. Miroshnyk I, Mirza S, Sandler N.2009. Pharmaceutical co-crystals-an opportunity for drug product enhancement. Expert opinion on drug delivery 6(4):333–341.

6. Caira MR.2007. Sulfa drugs as model cocrystal formers. Molecular pharmaceutics 4(3):310–316.

7. Alhalaweh A, Kaialy W, Buckton G, Gill H, Nokhodchi A, Velaga SP. 2013. Theophylline cocrystals prepared by spray drying: physicochemical properties and aerosolization performance. AAPS PharmSciTech 14(1):265–276.

8. Lover MJ. 1987. Use of 4-aminosalicylic acid as an anti-inflammatory agent. EP 0062000 B1 Patent.

9. Caira MR. 1992. Molecular complexes of sulphonamides 2. 1:1 complexes between drug molecules: sulfadimidine-acetylsalicylic acid and sulfadimidine-4-aminosalicylic acid. J Crystallogr Spectrosc Res 22:193–200.

10. Macrae CF, Bruno IJ, Chisholm JA, Edgington PR, McCabe P, Pidcock E, Rodriguez-Monge L, Taylor R, van de Streek J, Wood PA. 2008. Mercury CSD 2.0. New Features for the Visualization and Investigation of Crystal Structures. J Appl Cryst 41:466–470.

11. Tajber L, Corrigan OI, Healy AM. 2005. Physicochemical evaluation of PVP-thiazide diuretic interactions in co-spray-dried composites--analysis of glass transition composition relationships. European journal of pharmaceutical sciences : official journal of the European Federation for Pharmaceutical Sciences 24(5):553–563.

12. Bruker. 2007. TOPAS. Version 4.2. BRUKER AXS Madison, Wisconsin, USA.

13. David WIF, Shankland K, van de Streek J, Pidcock E, Motherwell WDS, Cole JC. 2006. DASH: A program for Crystal Structure Determination from Powder Diffraction Data. J. Appl. Cryst. 39:910–915.

14. Coelho AA. 2003. Indexing of powder diffraction patterns by iterative use of singular value decomposition. J. Appl. Cryst. 36:86–95.

15. Rietveld HM. 1969. A Profile Refinement Method for Nuclear and Magnetic Structures. J. Appl. Cryst. 2:65–71.

16. Le Bail A, Duroy H, Fourquet JL. 1988. Ab-initio structure determination of LiSbWO6 by X Ray powder diffraction. Mater. Res. Bull. 23:447–452.

17. Cheary RW, Coelho AA, Cline JP. 2007. Fundamental parameters line profile fitting in laboratory diffractometers. J Res Nat Inst Stand Technol 109:1–25.

18. Wermuth CG. 2008. The Practice of Medicinal Chemistry, 3rd Ed. Elsevier, Ltd.750.

19. Forbes RT, York P, Davidson JR. 1995. Dissolution kinetics and solubilities of p-aminosalicylic acid and its salts. International journal of pharmaceutics 126:199–208.

20. Good DJ, Rodríguez-Hornedo N. 2009. Solubility advantage of pharmaceutical cocrystals. Cryst Growth Des 9:2252–2264.

21. Grossjohann C, Eccles KS, Maguire AR, Lawrence SE, Tajber L, Corrigan OI, Healy AM. 2012. Characterisation, solubility and intrinsic dissolution behaviour of benzamide: dibenzyl sulfoxide cocrystal. International journal of pharmaceutics 422(1-2):24–32.

22. Healy AM, Corrigan OI. 1996. The influence of excipient particle size, solubility and acid strength on the dissolution of an acidic drug from two-component compacts. International journal of pharmaceutics 143:211–221.

23. Loureiro JM, Costa BFO, Le Caër G, Delcroix P. 2009. Partial amorphization of an α-FeCr alloy by ball-milling. Hyperfine Interactions 183:109–115.

24. Bhatt J, Murty BS. 2008. On the conditions for the synthesis of bulk metallic glasses by mechanical alloying. J Alloys Compd 459:135–141.

25. Caira MR, Nassimbeni LR, Wildervanck AF. 1995. Selective formation of hydrogen bonded cocrystals between a sulfonamide and aromatic carboxylic acids in the solid state. J Chem Soc Perkin Trans 2:2213–2216.

26. Karki S, Friscic T, Jones W, Motherwell WD. 2007. Screening for pharmaceutical cocrystal hydrates via neat and liquid-assisted grinding. Molecular pharmaceutics 4(3):347–354.

27. Friščić T, Jones W. 2009. Recent advances in understanding the mechanism of cocrystal formatin via grinding. Cryst Growth Des 9:1621–1637.

28. Apperley DC, Harris RK, Hodgkinson P. 2012. Solid State NMR: Basic Principles & Practice. ed., New York, USA: Momentum Press.

29. Lapidus SH, Stephens PW, Arora KK, Shattock TR, Zaworotko MJ. 2010. A Comparison of Cocrystal Structure Solutions from Powder and Single Crystal Techniques. Cryst Growth Des 10:4630–4637.

30. Wahl H, Haynes DA, le Roex T. 2012. Porous salts based on the pamoate ion. Chem. Commun. 48:1775-1777.

31. Wahl H, Haynes DA, le Roex T. 2011. Solvate formation in lutidinium pamoate salts: a systematic study. Cryst. Eng. Comm. 13:2227-2236.

32. Bethune SJ, Huang N, Jayasankar A, Rodríguez-Hornedo N. 2009. Understanding and Predicting the Effect of Cocrystal Components and pH on Cocrystal Solubility. Cryst Growth Des 9:3976–3988.

33. Nehm SJ, Rodríguez-Spong B, Rodríguez-Hornedo N. 2006. Phase solubility diagrams of cocrystals are explained by solubility product and solution complexation. Cryst. Growth Des. 6:592–600.

34. Murikipudi V, Gupta P, Sihorkar V. 2013. Efficient throughput method for hygroscopicity classification of active and inactive pharmaceutical ingredients by water vapor sorption analysis, Pharm. Dev. Technol. 18:348–358.